Available online at www.sciencedirect.com

ScienceDirect

Procedia Structural Integrity 28 (2020) 253–265

Structural Integrity Procedia

www.elsevier.com/locate/procedia

1st Virtual European Conference on Fracture

Evaluation of fatigue crack propagation in steel ESET specimens subjected to variable load spectra

Wim De Waele[a,*], Sven Trogh[a], Steven De Tender[a], Nahuel Micone[a], Kris Hectors[a,b],

[a] *Ghent University, Faculty of Engineering and Architecture, Department of Electromechanical, Systems and Metals Engineering, Laboratory Soete, Belgium*

[b] *SIM vzw, Tech Lane Ghent Science Park / Campus A 48, BE-9052, Zwijnaarde, Belgium*

Abstract

This paper reports on an experimental study of fatigue crack growth in steel specimens. First, block loading tests (sequences of low and high stress intensity factor ranges ΔK) are discussed. Limited crack growth retardation occurs at transitions from low to high load ranges; significant retardation or crack arrest are observed in high-low transitions. Next, semi-random load spectra are created, processed using a peak-and-valley analysis and further reduced by removing the load ranges below the stress intensity factor threshold ΔK_{th}. Rainflow counting is performed to obtain load profiles consisting of a sequence of blocks with constant ΔK. For the semi-random and the (reduced) peak-and-valley spectra no significant load interaction is observed. Pronounced crack growth retardation is observed in an ordered spectrum obtained by rainflow counting. The strong reduction in number of cycles of the (reduced) peak-and-valley spectra allows for exploration of accelerated fatigue testing. Experimental results of fatigue crack propagation are compared to results of calculations using a Python based numerical framework.

Keywords: Fatigue; Crack growth; variable amplitude, load sequence, load interaction

* Corresponding author.
E-mail address: Wim.DeWaele@ugent.be

2452-3216
10.1016/j.prostr.2020.10.031

1. Introduction

Machine components and engineering structures used in different industries are subjected to dynamically varying mechanical loads. For example, the loads exerted on offshore foundations of wind turbines find their origin in wind, currents and waves. When a structural flaw is present, the structure might eventually fail from fatigue crack growth originating at the flaw. The variable nature of the loads can lead to non-linear fatigue behavior as a consequence of load sequence and load interaction effects. These effects influence the crack growth rate and thus how fatigue damage accumulates (Pereira et al. 2008).

The effects of load interaction on fatigue crack growth can be evaluated by means of fatigue tests performed in a laboratory environment. It is, however, very challenging to accurately replicate service loads that are characterized by variable amplitude, variable load ratio or variable frequency. In order to shorten the test and reduce the complexity of fatigue testing, service load histories are often replaced by more simplified loading scenarios. In essence, the most extreme form of simplifying a service load, is to reduce it to a constant amplitude spectrum. This will however result in loss of load sequence and load interaction effects and cannot be representative for the real service load. If the reduced loading history leads to a more conservative fatigue life expectation, this method can be considered as a safe way of investigating. However, from an economical point of view, material could be saved by increasing the precision of fatigue life.

In order to evaluate load sequence effects, various block loading test programs have been performed (Sullivan and Crooker 1976), (Micone and De Waele 2019). Load sequence effects refer to the difference in (non-linear) damage accumulation during so-called low-high or high-low load sequences. A low-high load sequence is a load history represented by a succession of load blocks with increasing load range. A deviation from constant amplitude loading can give rise to acceleration or retardation of crack growth, called load interaction effects (Skorupa 1998). These load interaction effects have been studied by applying (combinations of) overloads or underloads during constant amplitude fatigue testing.

The fatigue crack growth rate da/dN, with a the crack length and N the number of cycles, is a function of the stress intensity factor range ΔK and the load ratio $R = K_{min}/K_{max}$. Under varying load conditions, also the previous loads (i.e. load history) will affect the crack growth rate. Crack growth acceleration or retardation can occur due to a deviation from a constant amplitude load sequence, i.e. when overloads or underloads happen. Loads deviating from constant amplitude may introduce compressive or tensile residual stress fields around a flaw tip and are thereby able to affect future crack growth rates. Load interaction effects make the prediction of fatigue life under variable amplitude loading much more complex than under constant amplitude loading. In practice, service loads might be so random that interaction effects either cancel out or become very unpredictable. Several researchers have performed studies using fatigue tests including underloads and overloads to gain more insight in the basic concepts of load interaction. Literature reviews on load interaction effects due to singular under- or overloads, sequence of under- or overloads and block loading sequences have been reported in (Schijve 1973), (Skorupa 1998, 1999) and (Laseure et al. 2015) amongst others. Especially, the effect of overloads has been extensively researched. It is generally accepted that tensile overloads result in crack growth retardation or could in some cases even lead to crack arrest. When applying an overload, there is a short initial acceleration in growth followed by a delay in crack growth after which the crack growth rate will reestablish to its steady state. A widely accepted physical explanation for the crack growth retardation is the theory of plasticity induced crack closure. This phenomenon of plasticity induced crack closure is associated with the development of residual plastically deformed material on the flanks of an advancing fatigue crack as discussed by Pippan and Hohenwarter (Pippan and Hohenwarter 2017). Tensile underloads have been studied to a lesser extent, but are known to be able to produce an increase in crack growth or crack growth acceleration. An illustration of different scenarios of load interaction, mostly leading to crack growth retardation, is shown in figure 1.

This paper is organized as follows. First, details on the test specimens and their instrumentation are reported. Next, an overview of the variable load spectra used for fatigue testing, i.e. two different block loading schemes and three sets of load spectra based on randomized load profiles. The subsequent section reports and discusses the results obtained from the different fatigue tests and also compares results with numerical predictions of fatigue crack length. Finally the paper is closed with a summary of the main conclusions.

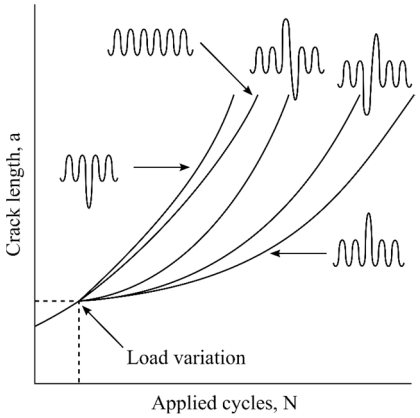

Figure 1: Typical crack growth evolution under several combinations of overload and underload cycles (Ribeiro et al. 2010)

2. Materials and Methods

2.1. Test specimens

For this study, eccentrically-loaded single edge crack tension specimens (ESET) have been subjected to fatigue loading. The geometry and dimensions of the ESET specimens are in accordance with standard ASTM E647 (ASTM 2015) and are illustrated in figure 2. A starter notch is introduced by milling followed by fatigue pre-cracking. The ESET specimens were extracted from a steel pipe with mechanical properties similar to the offshore steel grade NV F460 (Micone and De Waele 2019). The main strength and fatigue properties of this steel grade are summarized in table 1.

Table 1: Relevant properties of the NV F460 steel grade

σ_v [MPa]	σ_{UTS} [MPa]	C	m	ΔK_{th} [MPa√m]
560	635	3.6E-12	3.064	5.0

In the above table, σ_y and σ_{UTS} are the minimum specified yield stress and ultimate tensile strength respectively, C and m are, respectively, the experimentally determined coefficient and exponent of the Paris equation characterizing the fatigue crack growth rate:

$$\frac{da}{dN} = C\Delta K^m \tag{1}$$

ΔK_{th} is the threshold value for the stress intensity factor range; below this value no fatigue crack growth was observed. The stress intensity factor range (in MPa√m) is a function of the applied load and the specimen configuration; it can be expressed as

$$\Delta K = \frac{\Delta P}{B\sqrt{W}}F \tag{2}$$

with ΔP the load range, B the thickness of the specimen, W the width of the specimen and F a shape factor depending on the relative crack size a/W defined in [9].

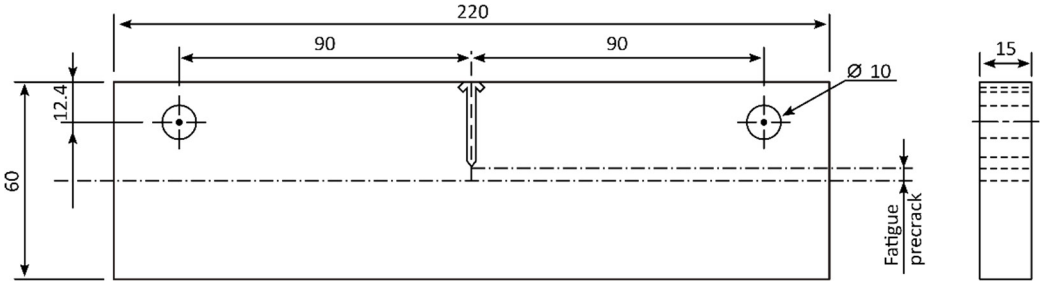

Figure 2: Schematic illustration of ESET specimen extracted from a pipe made of offshore steel grade NV F460.

2.2. Instrumentation

The main goal of this study is to quantify the fatigue crack growth (rate) during the long crack propagation phase of variable load amplitude tests. All fatigue tests have been performed on an MTS810 servo-hydraulic test machine with a load cell capacity of 100kN. The tests were performed in force controlled mode at a loading frequency of 10Hz. On-line determination of fatigue crack growth has been determined by the compliance technique using clip gauge measurements. An instrumented test specimen is shown in figure 3. This photograph also shows different electrical wires that were used for measurement of crack length using the direct current potential drop (DCPD) technique (De Tender, Micone, and De Waele 2016).The DCPD measurements are not further reported in this paper.

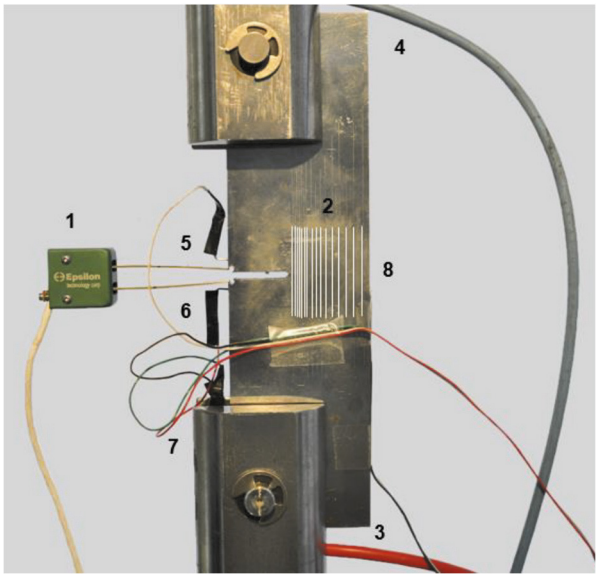

Figure 3: Photograph of an instrumented ESET specimen: (1) clip gauge, (2) marker lines, (3,4) input wires for direct electrical current, (5-6) DCPD probes, (7) reference probes to compensate for environmental effects, (8) back face electrical strain gauge.

A clip gauge (type Epsilon 3541-005M-100M-LT with 5mm gauge length) mounted at the crack mouth is used to measure the crack mouth opening displacement (CMOD) from which the relative crack depth can be calculated using the following compliance equation:

$$\frac{a}{W} = M_0 + M_1 U + M_2 U^2 + M_3 U^3 + M_4 U^4 + M_5 U^5 \tag{3}$$

with M_i constants defined in [9]. Variable U is calculated as

$$U = \left[\sqrt{\frac{EB\Delta v_0}{\Delta P}} + 1 \right]^{-1} \tag{4}$$

with E the Young's modulus and Δv_0 the CMOD range during one fatigue cycle with load range ΔP.

The clip gauge results have been validated by means of visual inspection using marker lines scratched on the surface (see figure 4) and a microscope camera.

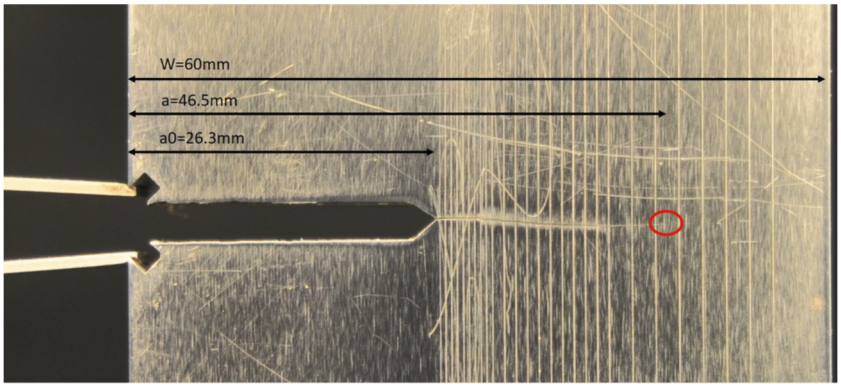

Figure 4: Detail of ESET specimen showing the machined starter notch and the final fatigue crack length a=46.5mm.

2.3. Fatigue load profiles and spectra

The first series of experiments consists of two types of block loading tests. The block loading schemes comprise a sequence of low to high stress intensity factor ranges on the one hand and a sequence of low-high-low stress intensity factor ranges on the other hand. These block loading schemes are illustrated in figure 5. Next, three sets of fatigue spectra were created for this study. For the first set, a load profile consisting of 400 stress intensity factor range values randomly selected from five possible values, further called random profile, is defined and repeated 2000 times to create a reference semi-random fatigue load spectrum. The random load profile is then used to create three different and shorter load profiles. First the random load profile is reduced to 236 load values by means of a peak-and-valley analysis. A further reduction is obtained by removing all load cycles corresponding to a stress intensity factor range below the material's threshold value ΔK_{th}=5MPa$\sqrt{m}$. The reason being that these cycles are expected to have a negligible influence on the total fatigue crack growth. This reduced peak-and-valley load profile consists of 196 load values. The fourth and final fatigue spectrum is obtained by a rainflow counting analysis performed on the peak-and-valley load profile. The result is a load profile with identical length but with the load values arranged according to decreasing ΔK ranges. These load profiles are illustrated in figure 6.

For sets 2 and 3, two additional random load profiles were created by using the same stress intensity factor ranges but increasing the number of load values with a factor 10 and 100 respectively. These random load profiles are repeated 200 and 20 times respectively, resulting in semi-random load spectra of a similar length to the spectrum defined for set 1. For these load profiles, again peak-and-valley analysis and rainflow counting are performed to define additional load spectra. An overview of all load spectra that have been used for fatigue testing, is given in table 2.

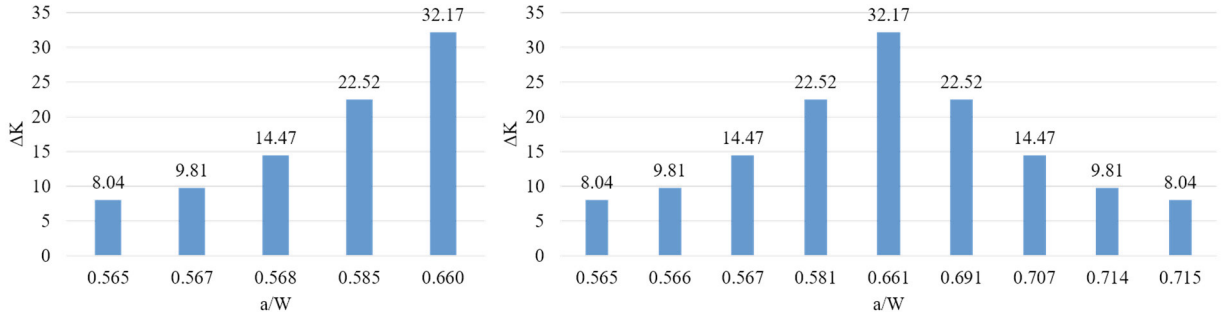

Figure 5: Block loading tests performed on ESET specimens; low-high sequence of stress intensity factor ranges (left) and low-high-low sequence (right).

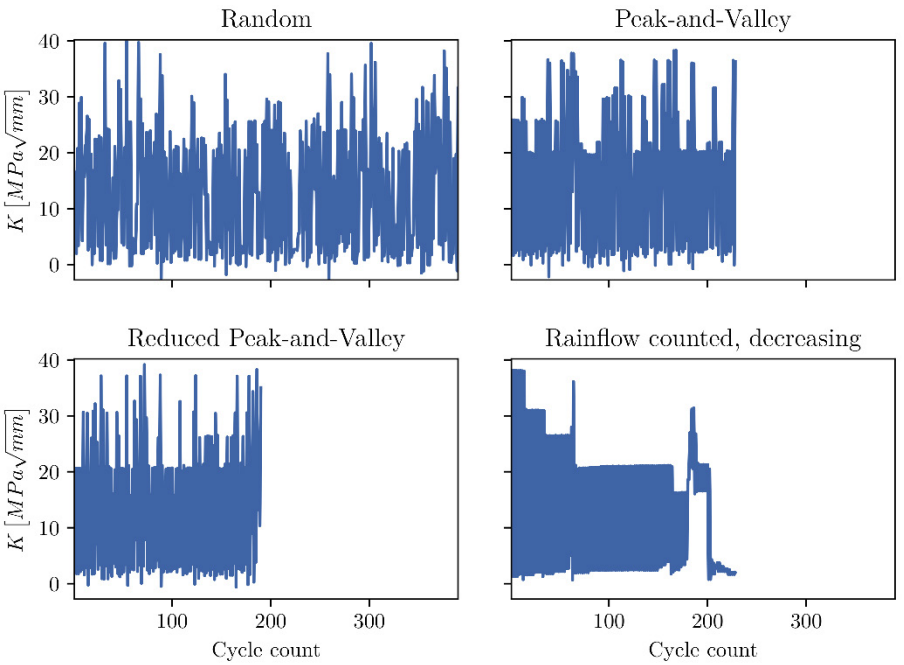

Figure 6: Illustration of four load profiles: (a) random profile based on 400 stress intensity factor range values, (b) peak-and-valley profile consisting of 236 stress intensity factor range values, (c) reduced peak-and-valley profile consisting of 196 stress intensity factor range values, and (d) profile obtained after rainflow counting of the peak-and-valley profile and blocks arranged according to decreasing load ranges.

Table 2: Overview of spectra created as repetitions of load profiles

	Profile repetitions	Random profile	Peak-and-valley & rainflow counted profiles	Reduced peak-and-valley
			[number of load values]	
Set 1	2000	400	236	196
Set 2	200	4000	2369	2105
Set 3	20	40000	23978	18453

3. Experimental Results

3.1. Block loading

The results of a low-high block loading scheme with constant stress intensity factor range for each of five load blocks is shown in figure 7. All points represent *da/dN* measurements taken during the test for different Δ*K* blocks; the different colours refer to the different Δ*K* values. The horizontal dash-dotted lines in the figure give an indication of the expected crack growth rate based on the experimentally determined Paris law curve of the material. Based on figure 7, it can be concluded that a small amount of crack growth rate retardation occurs going from a lower Δ*K* value to a higher one. Besides, it can be concluded that the retardation is more pronounced for lower Δ*K* values than for the higher ones. For the highest Δ*K* no retardation can be observed.

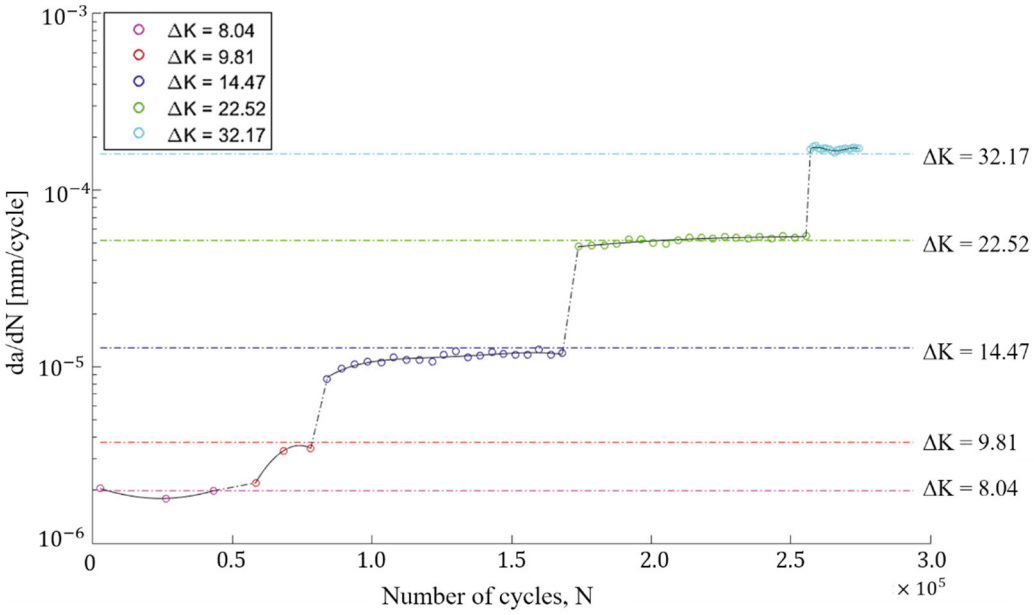

Figure 7: Crack growth rate measured during a low-high block loading scheme performed on an ESET specimen (De Tender 2016).

Figure 8 shows similar results for a low-high-low block load test. At the start of the test the clip gauge measurements were not stable, resulting in significant scatter in the crack growth rate *da/dN*. In the low-high part of the test a slight crack growth rate retardation is observed at the transition from $\Delta K = 14.47\ MPa\sqrt{m}$ to $\Delta K =$

22.52 $MPa\sqrt{m}$. The evolution in *da/dN* values reveals a significant retardation effect during the high-low part of the test. After the first transition ($\Delta K = 32.17\ MPa\sqrt{m}$ to $\Delta K = 22.52\ MPa\sqrt{m}$) the crack growth rate eventually goes back to the value predicted from the Paris law curve. The next transition to $\Delta K = 14.47\ MPa\sqrt{m}$ causes an even higher retardation effect and the crack growth rate does not return to its predicted value. Upon the transition to 9.81MPa√m, crack arrest occurred and therefore no further *da/dN* measurement points are shown.

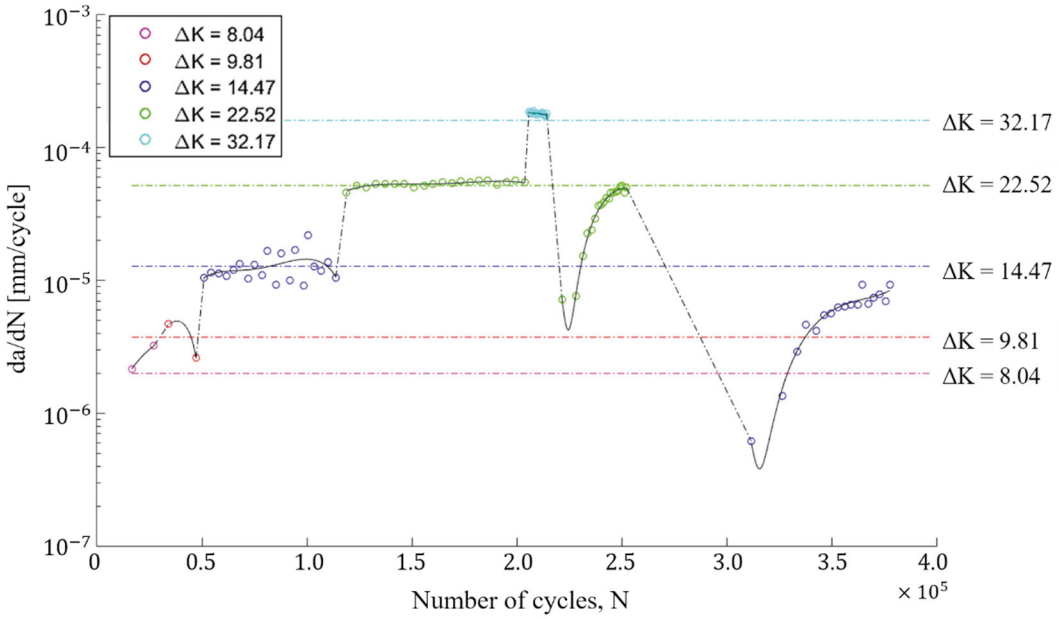

Figure 8: Crack growth rate measured during a low-high-low block loading scheme performed on an ESET specimen (De Tender 2016).

3.2. Random, peak-and-valley and reduced peak-and-valley load profiles

The experimental results for the load spectra based on the randomized load profiles of sets 1, 2 and 3 are shown in figure 9. The evolution of all three fatigue crack growth curves is continuously increasing; the small spikes on the crack growth curves can most probably not entirely be assigned to signal noise but indicate local load interaction effects due to high-low and low-high transitions. It is hypothesized that for the random load spectra, the load interaction effects (i.e. crack growth retardation and crack growth acceleration) more or less compensate each other. For the peak-and-valley and reduced peak-and-valley spectra the experimentally observed fatigue crack growth curves also showed a continuous evolution. The final fatigue crack length measured for the semi-random load spectra increases with increasing number of load profile repetitions (i.e. for shorter load profiles).

3.3. Rainflow counted load profiles

The rainflow counting algorithm results in an ordered load profile and based on the results of the preliminary block loading tests is expected to reveal pronounced load sequence and interaction effects. Depending on the number of profile repetitions needed to generate the complete load spectrum, the load interaction effects and the total fatigue crack growth can differ. The experimental results are shown on figure 10 and are also compared to numerical predictions based on the classical Paris equation, which does not account for load interaction effects and also does not

account for load ratio effects. The experimental curves were obtained using a digital filter (type Savitzky-Golay) that smoothens the raw data and therefore only show the global evolution of fatigue crack growth; this is because the non-filtered data contain a lot of load interaction events (figure 12) leading to an ambiguous representation of the data. For the longest load profile with the lowest number of repetitions, corresponding to set 3, the experimental crack growth rate is clearly slower than the results of set 2 and 3, illustrating the most pronounced influence of global crack growth retardation (see figure 10). This could be expected as a larger number of repetitions leads to a more random nature of the total load spectrum. The differences between the experimental crack growth values and the values calculated using the Paris equation are significant for the load spectra of set 1 and set 3. The relative deviation between the experimental and numerical values is maximal for set 3, i.e. the experiment showing the highest crack growth retardation effect.

An overview of all experimentally determined final fatigue crack lengths for the different load spectra is given in table 3. Also shown are the results of the numerical simulations for the load spectrum of set 3 obtained after rainflow counting of the peak-and-valley load profile. Focusing on the experimental values, there is an observable difference in final fatigue crack growth between the randomized load spectrum and the rainflow counted spectrum for sets 2 and 3. For set 1, having the largest number of load profile repetitions, the difference between crack growth of the randomized spectrum and the rainflow counted spectrum is very low. Reducing a random load spectrum by peak-and-valley analysis and subsequent ordering by rainflow counting has an important influence on fatigue crack growth.

Table 3: Overview of final fatigue crack length for different load spectra obtained by experiments and numerical calculations

	Set 1 (2000 repetitions)	Set 2 (200 repetitions)	Set 3 (20 repetitions)
		Random load profiles	
Δa_{exp} [mm]	10.07	8.81	10.49
		Peak-and-valley profiles	
Δa_{exp} [mm]	9.94	6.78	6.63
		Reduced peak-and-valley profiles	
Δa_{exp} [mm]	10.49	6.09	6.55
		Rainflow counted spectra	
Δa_{exp} [mm]	9.63	4.62	3.74
		Δa_{Paris} [mm]	6.15
		$\Delta a_{Willenborg}$ [mm]	3.96
		$\Delta a_{Wheeler}$ [mm]	1.49

4. Accelerated fatigue crack growth testing

Accelerated fatigue testing can be performed by increasing test frequency, increasing load or reducing load spectra by removing non-damaging load cycles. In this study, the authors evaluate the effect of reducing the number of load cycles on the final fatigue crack growth. The reduction of number of cycles is performed in two steps, first by peak-and-valley analysis and second by also removing the load cycles with a stress intensity factor range below the threshold value. The results reported in table 3 reveal that, also considering the inherent scatter in fatigue data, the difference in crack growth between peak-and-valley and reduced peak-and-valley spectra is limited. Removing the load cycles with ΔK values below the threshold thus has a negligible effect on final crack growth and reduces the fatigue test duration. The peak-and-valley analysis however leads to a significant decrease in fatigue crack growth for sets 2 and 3. Only for set 1, i.e. having the largest number of profile repetitions, the different load spectra lead to similar fatigue crack growth as illustrated on figure 11.

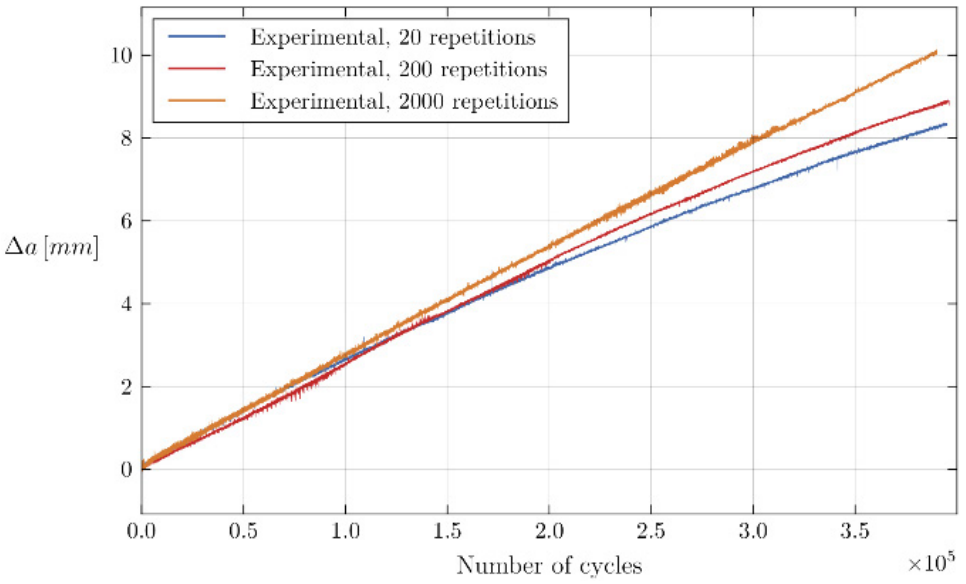

Figure 9: Evolution of fatigue crack growth for experiments based on random load profiles.

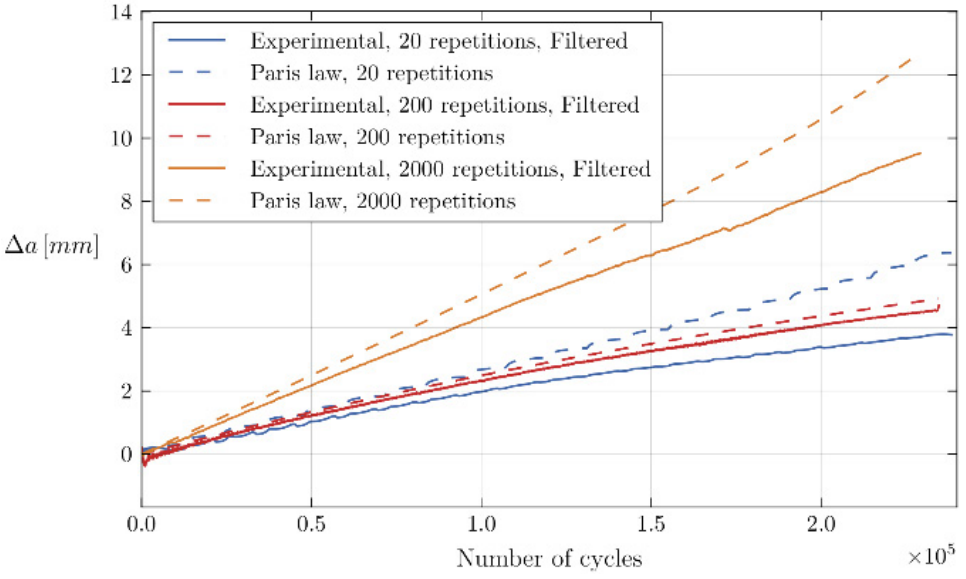

Figure 10: Influence of load profile length on fatigue crack growth for rainflow counted spectra. Experimentally determined values are compared to numerical predictions based on the Paris equation.

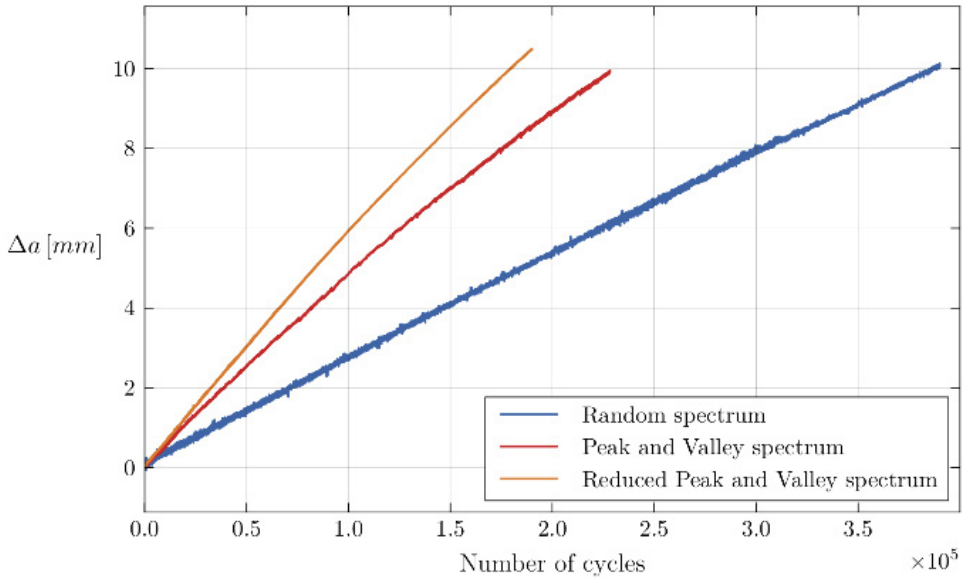

Figure 11: Evolution of experimentally determined fatigue crack growth for three load spectra of set 1 (highest number of repetitions). The peak-and-valley and reduced peak-and-valley spectra allow to significantly reduce test duration whilst reaching a comparable final fatigue crack length.

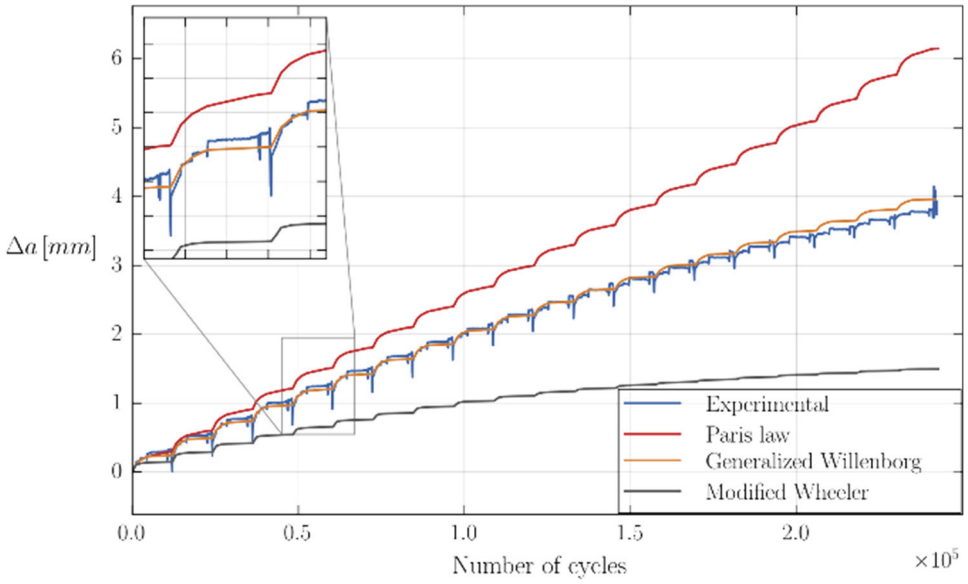

Figure 12: Evolution of the experimentally determined fatigue crack growth during a load spectrum consisting of 20 repetitions of a rainflow counted load profile and comparison with numerical results obtained with the Paris equation not considering load interaction, and the modified Wheeler and generalized Willenborg models that take crack retardation into account.

5. Numerical results

Because global crack retardation is most significant in the results of the rainflow counted spectrum of set 3, the experimental data of this load spectrum are used for comparison with numerical predictions (table 3) using an in-house developed Python based numerical framework (Muys et al. 2017; Zhang et al. 2019).This framework is able to perform cycle-by-cycle fatigue crack growth simulations using different crack growth functions (Paris, Walker, Wheeler, Willenborg) and was developed to study load interaction effects. The inputs of the numerical framework are the actually applied forces P logged during the fatigue tests. The actually applied forces differ slightly from the programmed load spectrum and in order to obtain the most accurate simulations the actual (i.e. not the programmed load spectra) load spectra were used. From this data (P_{min} and P_{max} of each cycle) the stress intensity factor ranges ΔK and load ratios R can be calculated.

Prediction of fatigue crack growth based on the Paris equation largely overestimates the experimentally measured fatigue crack growth for the rainflow counted load spectrum. This equation does not account for load interaction effects and its predictions are therefore indeed expected to deviate significantly from experimental values for load cases exhibiting significant crack retardation. The parameters used for the Paris equation are those reported in table 1. These parameters are the average values obtained from three fatigue tests at a load ratio 0.1. Although the load ratio R is not constant throughout the experiments, constant values for the Paris coefficient and for the Paris exponent are used. This is due to the lack of experimental data for other load ratios and further motivated because it is generally accepted that the Paris parameter C is a function of R but the slope of the Paris curve is almost constant (Huang and Moan 2007).

To numerically evaluate load interaction effects, plastic zone models based on the original Wheeler (Wheeler 1972) and Willenborg (Willenborg 1971) models have been implemented in the numerical framework. These plastic zone models were developed to account for crack growth retardation; their basic principles are discussed in (Zhang et al. 2019). In short, when an overload is applied, a plastic zone is created which will retard the fatigue crack growth rate if the plastic zone size of the next load is smaller than the reference plastic zone size. The numerical predictions have been obtained using a modified Wheeler model and a generalized version of the Willenborg model (Muys et al. 2017). As can be observed from figure 12, the simulations using the generalized Willenborg model generate a crack growth evolution that is almost identical to the experimentally measured crack growth. The Paris law, ignoring load retardation, overestimates the experimental crack growth whilst the Wheeler model seriously underestimates the experimental data.

The fatigue crack growth curves, experimental and numerical ones, in figure 12 clearly indicate a periodicity corresponding to the repetitions of the load profiles. A detailed view is shown in the top left of the figure. The experimental curve clearly presents global crack growth retardation and sudden crack growth acceleration during each load profile. It also contains physically impossible events, i.e. sudden drops in fatigue crack length. Taking into account that these events are repeated in all load profile repetitions, they should not be attributed to signal noise. It has to be recalled that the fatigue crack length is calculated based on a measurement of the crack mouth opening. A decrease in calculated crack length is therefore the result of a decrease in crack mouth opening and this can most probably be attributed to a crack closure effect resulting from plastic zone development at the crack tip due to an overload.

6. Conclusions

ESET specimens made of an offshore steel grade have been subjected to variable load spectra. Fatigue crack growth in these ESET specimens has been calculated using online measurement of crack mouth opening displacement and the compliance method. Two block loading tests, one sequence of low-high and one sequence of low-high-low ΔK values, have first been performed. In both tests limited crack growth retardation has been observed at the transition from low to high ΔK blocks. The transitions from high to low ΔK blocks revealed significant amounts of crack growth retardation and even crack arrest.

Three semi-random load spectra have been created as a repetition of random load profiles with different lengths and have been processed using a peak-and-valley analysis and further reduced by removing the load ranges below ΔK_{th}. Ordered load profiles have been created by rainflow counting of the random profiles and arranging the blocks according to decreasing stress intensity factor range. Effects of load interaction on the overall evolution of fatigue crack growth has not been observed for the semi-random, the peak-and-valley and the reduced peak-and-valley spectra. The strong reduction in number of cycles of the (reduced) peak-and-valley spectra have revealed their potential for accelerated fatigue testing, i.e. significantly reducing test duration whilst reaching a comparable final fatigue crack length. The most pronounced crack growth retardation has been observed for the ordered spectrum obtained by rainflow counting and having the least amount of repetitions.

Experimental results of fatigue crack propagation have finally been compared to results of calculations using a Python based numerical framework including the conventional Paris equation and plastic zone models according to Wheeler and Willenborg that allow to include the effects of crack growth retardation. The generalized Willenborg model was able to accurately predict the fatigue crack growth observed in the experiment showing a pronounced effect of retardation. The predictions based on the Paris equation and the Wheeler model overestimated and underestimated the final fatigue crack length respectively.

7. Acknowledgments

Kris Hectors acknowledges the financial support of Vlaio through the SafeLife project (project number 179P04718W) and also the support of SIM (Strategic Initiative Materials in Flanders) and IBN Offshore Energy.

8. References

ASTM. 2015. “E647-15e1, Standard Test Method for Measurement of Fatigue Crack Growth Rates.”

Huang, Xiaoping and Torgeir Moan. 2007. “Improved Modeling of the Effect of R-Ratio on Crack Growth Rate.” *International Journal of Fatigue* 29(4):591–602.

Laseure, Niels, Ingmar Schepens, Nahuel Micone, and Wim De Waele. 2015. “Effects of Variable Amplitude Loading on Fatigue Life.” *International Journal Sustainable Construction & Design* 6(3):10.

Micone, N. and W. De Waele. 2019. “Experimental Evaluation of Block Loading Effects on Fatigue Crack Growth in Offshore Structural Steels.” *Marine Structures* 64(October 2018):463–80.

Muys, L., J. Zhang, N. Micone, W. De Waele, and S. Hertelé. 2017. “Cycle-by-Cycle Simulation of Variable Amplitude Fatigue Crack Propagation.” *Sustainable Construction and Design* 8(1):8.

Pereira, H. F. S. G., A. M. P. de Jesus, A. A. Fernandes, and A. S. Ribeiro. 2008. “Analysis of Fatigue Damage under Block Loading in a Low Carbon Steel.” *Strain* 44(6):429–39.

Pippan, R. and A. Hohenwarter. 2017. “Fatigue Crack Closure: A Review of the Physical Phenomena.” *Fatigue and Fracture of Engineering Materials and Structures* 40(4):471–95.

Ribeiro, A. S., A. P. Jesus, J. M. Costa, L. P. Borrego, and J. C. Maeiro. 2010. “Variable Amplitude Fatigue Crack Growth Modelling.” *Revista Da Associação Portuguesa de Análise Experimental de Tensões ISSN 1646* 19:33–44.

Schijve, J. 1973. “Effect of Load Sequences on Crack Propagation under Random and Program Loading.” *Engineering Fracture Mechanics* 5(2):269–80.

Skorupa, M. 1998. “Load Interaction Effects during Fatigue Crack Growth under Variable Amplitude Loading-a Literature Review. Part I: Empirical Trends.” *Fatigue and Fracture of Engineering Materials and Structures* 21(8):987–1006.

Skorupa, M. 1999. “Load Interaction Effects during Fatigue Crack Growth under Variable Amplitude Loading - a Literature Review. Part II: Qualitative Interpretation.” *Fatigue and Fracture of Engineering Materials and Structures* 22(10):905–26.

Sullivan, A. M. and T. W. Crooker. 1976. “Analysis of Fatigue-Crack Growth in a High-Strength Steel—Part II: Variable Amplitude Block Loading Effects.”

De Tender, Steven. 2016. “Variable Amplitude Fatigue in Offshore Structures.”

De Tender, Steven, Nahuel Micone, and Wim De Waele. 2016. “Online Fatigue Crack Growth Monitoring with Clip Gauge and Direct Current Potential Drop.” *International Journal Sustainable Construction & Design* 7(1):6.

Wheeler, Orville Eugene. 1972. “Spectrum Loading and Crack Growth.”

Willenborg, J. 1971. “A Crack Growth Retardation Model Using an Effective Stress Intensity Concept.” *Technical Report*.

Zhang, Jie, Louis Muys, Steven De Tender, Nahuel Micone, Stijn Hertelé, and Wim De Waele. 2019. “Constraint Corrected Cycle-by-Cycle Analysis of Crack Growth Retardation under Variable Amplitude Fatigue Loading.” *International Journal of Fatigue* 125(April):199–209.